Region-based Vessel Segmentation Using Level Set Framework

Gang Yu, Pan Lin, Peng Li, and Zhengzhong Bian

Abstract: This paper presents a novel region-based snake method for vessel segmentation. According to geometric shape analysis of the vessel structure with different scale, an efficient statistical estimation of vessel branches is introduced into the energy objective function, which applies not only the vessel intensity information, but also geometric information of line-like structure in the image. The defined energy function is minimized using the gradient descent method and a new region-based speed function is obtained, which is more accurate to the vessel structure and not sensitive to the initial condition. The narrow band algorithm in the level set framework implements the proposed method, the solution of which is steady. The segmentation experiments are shown on several images. Compared with other geometric active contour models, the proposed method is more efficient and robust.

Keywords: Energy function, level set, region-based segmentation, snake.

1. INTRODUCTION

Vessel segmentation is an important area in medical image processing. The extracted vessel features that help identify pathological changes are a prior step in the medical diagnosis automation because many diseases are accompanied with the change of vessel shape. Moreover, the vessel segmentation provides a tool to understand the relation between vessels and diseases.

The vessel segmentation methods were widely investigated in the past. Early conventional approaches for vessel segmentation are matched filter methods [1] and morphological methods [2]. In these approaches, detection accuracy and validity of post processing are undesirable. Sonka developed an efficient edge detector to compute the diameter of small coronary vessels [3]. Yuan developed an approach to detect the inner and outer boundaries of the blood vessel wall in MR images [4], but the algorithm is limited to normal carotid arteries. Zana presented an algorithm based on point correspondence for the registration of eye fundus images [5]. However, the initial matching may influence the algorithm complexity seriously.

Nowadays, active contour (snake) models [7,9-12] have become effective tools for extraction of the region of interests(ROI), which were widely investigated for overcoming the limitations of traditional methods. Sethian *et al.* first introduced the level set method into active contour models for numerical implementation [6]. In [7], it applied level-set-based active contour methods to vessels extraction, whose corresponding curve evolution is controlled by gradient information. The following boundary-based (or edge-based) approaches add the curvature term and advection term to evolution equation for smoothing the curve and driving the front into the desired boundary [13]. These investigations may improve the segmentation results, but the boundary-based speed function could not work well in low contrast or noise image, since the edge information is too weak there. Moreover, Most of the methods are sensitive to initial condition and all the seeds must be set nearby ROI. Region-based methods are more suitable for vessel segmentation because the global region information, including boundary gradient information, is considered. Yezzi proposed a fully global approach to image segmentation that is derived based on the global segmentation of an image. This is a pure region-based approach but it may bring expensive computational cost [10]. Region active contour models, such as the geodesic active region model presented by Nikos [9], which integrates boundary-based with region-based active contour approaches, are more effective snake-based segmentation methods, because prior knowledge about ROI is introduced in them [11,12].

The remainder of the paper is organized as follows.

Manuscript received June 19, 2005; revised December 5, 2005; accepted June 21, 2006. Recommended by Editorial Board member Hoon Kang under the direction of Editor Keum-Shik Hong. This work was supported by National Natural Science Foundation of China under grant No. 60271022, 60271025, and 30400110.

Gang Yu, Peng Li, and Zhengzhong Bian are with the School of Life Science and Technology, Xi'an Jiaotong University, Xi'an, Shannxi, 710049, China (e-mails: {yugang, lpdcy, bzzbme}@mailst.xjtu.edu.cn).

Pan Lin is with the Faculty of Software, Fujian Normal University, Fuzhou, Fujian, 350007, China (e-mail: linpan99@sohu.com).

In Section 2, the multiscale vessel analysis is introduced; in Section 3, the proposed vessel region information function is described and the new speed equation is developed; in Section 4, experiments are presented and compared with that of the existing active contour models; finally conclusions are reported.

2. MULTISCALE VESSEL ANALYSIS

The multiscale vessel enhancement filtering was presented in Reference [8]. The filter depends on the eigenvalues $\lambda_{\sigma,k}$ (k = 1,2,3; σ is the scale) of the Hessian Matrix of the second order image structure. The eigenvalues show the speed of intensity variation in the images. The correspondencing eigenvectors express three orthonormal directions: $u_{\sigma,1}$ indicates minimum intensity variation, i.e., the direction along the vessel. $u_{\sigma,2}$ and $u_{\sigma,3}$ are orthogonal to $u_{\sigma,1}$. The ideal tubular structure in 3D images is: $|\lambda_{\sigma,1}| \approx 0, |\lambda_{\sigma,1}| << |\lambda_{\sigma,2}|, \lambda_{\sigma,2} \approx \lambda_{\sigma,3}$. See Fig. 1.

Table 1 summarizes the relations that must hold between the eigenvalues of the Hessian Matrix for the detection of different structures.

Possible pattern in 3D depend on the value of the eigenvalues λ_k. H = high, L = low, N = noisy, +/- indicate the sign of the eigenvalues. Bright is bright vessel with dark background. Dark is dark vessel with bright background.

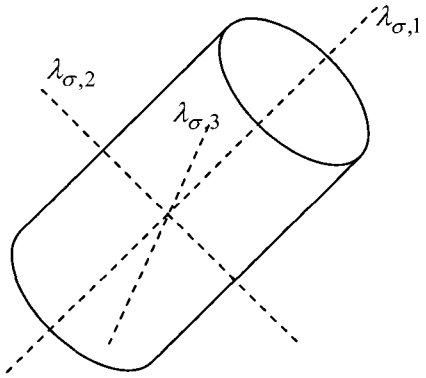

Fig. 1. Tubular structure and eigenvalues.

Table 1. Possible pattern and the eigenvalues.

3D			Pattern
λ_1	λ_2	λ_3	
N	N	N	Background/Noisy
L	L	H-	Plate-like(bright)
L	L	H+	Plate-like(dark)
L	H-	H-	Tubular (bright)
L	H+	H+	Tubular(dark)
H-	H-	H-	Blob-like(bright)
H+	H+	H+	Blob-like(dark)

Two basic ratios and a measure for distinguishing background are defined in Reference [8].

$$R_B = \frac{|\lambda_1|}{\sqrt{|\lambda_1\lambda_2|}}, \quad R_A = \frac{|\lambda_2|}{|\lambda_3|}, \quad S = \|H\|_F = \sqrt{\sum_{j\le D} \lambda_j^2}.$$

The first ratio accounts for the deviation from a blob-like structure but cannot distinguish between a line- and a plate-like pattern. The second ratio refers to the largest area cross section of the ellipsoid (in the plane orthogonal to $u_{\sigma,1}$). It is essential for distinguishing line-like from plate-like structures since only in the latter case it will be zero. The final measure s is the norm of eigenvalues of Hessian matrix. s will be low in the background where no structure is presented and the eigenvalues are small. The vessel-enhancement filter $v(x,\sigma)$ at location x and at scale σ is defined. The vesselness measure provided by the filter response at different scales can obtain a final estimate of the vesselness or vessel probability:

$$v(x,\sigma) = \begin{cases} 0 & \text{if } \lambda_2 > 0 \text{ or } \lambda_3 > 0 \\ (1-\exp(-\frac{R_A^2}{2\alpha^2}))\exp(-\frac{R_B^2}{2\beta^2})(1-\exp(-\frac{S^2}{2c^2})) \end{cases}$$

α, β, c are parameters, which control the sensitivity of the line filter to the measures. α, β are fixed to 0.5. The value of the threshold c depends on the grey-scale range of the image and half the value of the maximum Hessian norm has been proven to work in most cases [8]. The filter in 2D images can be reduced as:

$$v(x,\sigma) = \begin{cases} 0 & \text{if } \lambda_2 > 0 \\ \exp(-\frac{R_B^2}{2\beta^2})(1-\exp(-\frac{S^2}{2c^2})). \end{cases} \quad (1)$$

The filter is applied at multiple scales that span the range of expected vessel widths according to the image anatomy. The response of multiscale filter will be maximum at the scale that approximately matches the size of the vessel to detect. The response in mismatched scales is very small and may be sensitive to noise or be confused with the backgrounds. Therefore, the maximum response at the matched scale is applied to obtain a final estimate of vesselness or vessel probability:

$$v(x) = \max_{\sigma_{\min} \le \sigma \le \sigma_{\max}} v(\sigma, x). \quad (2)$$

Obviously, $v(x)$ is between 0 and 1. Equation (1) is given for bright curvilinear structures (Magnetic Resonance Angiography and Computed Tomography Angiography). For dark objects (as in Digital

Subtration Angiography), the conditions should be reversed. Multiscale filter is helpful to improve segmentation in noise images. Meanwhile, some small areas with big $v(x)$ should be excluded in real application because these areas are only possibly produced by serious noise, not real vessels.

3. VESSEL REGION INFORMATION FUNCTION AND EVOLUTION EQUATION

3.1. Vessel region estimation

The image segmentation can be viewed as an optimization problem with respect to a posteriori partition probability. Usually, the posteriori probability density function is given according to prior probability by the Bayes rule. The vesselness measure is maximal at the center of the vessel and decreases to zero at the vessel boundaries, which is suitable to be used as vessel probability estimation. For example, if the vesselness measure of a pixel is close to 1, it is likely that the pixel is in the vessels; otherwise it is out of the vessels. Therefore, we define the vessel region information function as:

$$P(I(x))=\begin{cases}1 & if\ \ v(x)\ge a\\ v(x) & if\ v(x)<a\ \ and\ \ v(x)\ge b\\ -(1-v(x)) & if\ v(x)<b,\end{cases} \tag{3}$$

where $a,b\in[0,1], I(x)$ is the image intensity, x is the location vector. a,b are parameters, which control the sensitivity of region information function. $a=0.4$, $b=0.2$ have proven to work well in most cases. $P(I(x))$ is a piecewise function, whose values range [-1,1]. When its value is 1 or close to 1, the voxel should be a point in the vessels. When its value is much smaller than 1, the voxel may be in or out of vessel. When the value of $P(I(x))$ is negative, the voxel is out of vessels. Moreover, the smaller the function value, the smaller the vessel probability. Therefore, $P(I(x))$ is equal to an efficient estimation of the vessel probability function, which applies not only vessel intensity information, but also the whole line-like structure information of vessels. Here, we extend the values range of probability function from [0,1] to [-1,1]. Note the sign of $P(I(x))$ may be negative, because we will apply it to the snake framework as a region-based external force or speed function (Section 3.2). The negative force makes the curve shrink.

3.2. Regionprobability d-based external force

The new energy objective function based on vessel region information in 3D space is presented as:

$$E_{vessel}=-\iint_R p(I(x,y,z))dxdydz, \tag{4}$$

where R is the interior fields of the curve (2D) or surface (3D). The integral in (4) is to find the boundary of R where E_{vessel} is minimized. The straightforward understanding to the equation is that the boundary of curve or surface should include voxels in the vessels as many as possible. Moreover, E_{vessel} is a region-based energy function and not sensitive to the initial condition.

Integrate it with boundary-based energy function; the whole energy function is described as:

$$E=\alpha E_{vessel}+(1-\alpha)E_{Boundary}, \tag{5}$$

where $\alpha\in[0,1]$.

In this paper, we choose geodesic active contour as boundary information energy. It is defined as:

$$E=\alpha E_{vessel}+(1-\alpha)\int_0^1 g\{|\nabla I(C)|\}|C'(p)|dp. \tag{6}$$

According to the variational theory and gradient descent method, we can acquire its evolution equation by minimizing E_{vessel}. See Appendix A. It is presented as:

$$\frac{\partial C}{\partial t}=p(I(x,y,z))\cdot\vec{N}, \tag{7}$$

where $\vec{N}$ is the outer normal vector of the curve or surface. When the curve is in the vessels, the vesselness measure tends to be big. Therefore, the evolution speed is equal or close to 1, which creates a large expansible force to make the convergence more rapid. When the curve is out of the vessels, the evolution speed is close to -1, which makes the curve shrink rapidly. In other cases, both vessel force and boundary force control the curve evolution.

Reference [13] presented the evolution equation of geodesic active contour. The geodesic active contour evolution model is:

$$\frac{\partial C}{\partial t}=g(|\nabla I|)(c_1+c_2k)\cdot\vec{N}-(\nabla g(|\nabla I|)\cdot\vec{N})\cdot\vec{N}, \tag{8}$$

where k is the curvature of curve, c_1, c_2 are parameters.

With (5), (7), and (8), the final speed function is defined as:

$$\begin{aligned}\frac{\partial C}{\partial t}&=\alpha\times p(I(x,y,z))\cdot\vec{N}+(1-\alpha)\\ &\quad\{g(|\nabla I|)(c_1+c_2k)\cdot\vec{N}-(\nabla g(|\nabla I|)\cdot\vec{N})\cdot\vec{N}\}.\end{aligned} \tag{9}$$

3.3. Evolution equation in level set framework

It is assumed that the curve C is a level set of a function of $u:[0,a]\times[0,b]\to R$. That is, C coincides

with the set of points u=constant. u is therefore an implicit representation of the curve C. This representation is parameter free.

If the planar curve C evolves according to

$$\frac{\partial C}{\partial t} = \beta \vec{N}$$

for a given speed function β, the embedding function u should deform according to

$$\frac{\partial u}{\partial t} = \beta |\nabla u|.$$

By embedding the evolution of C in that of u, topological changes of C are handled automatically and the accuracy and stability are achieved using the proper numerical algorithm.

Because of $\vec{N} = \frac{\nabla u}{|\nabla u|}$, the level set evolution equation from level set theory is:

$$\frac{\partial u}{\partial t} = \alpha \times p(I(x,y,z)) \cdot |\nabla u| + (1-\alpha) \{g(|\nabla I|)(c_1 + c_2 k) \cdot |\nabla u| - (\nabla g(|\nabla I|) \cdot \vec{N}) \cdot |\nabla u|\}, \quad (10)$$

where $k = div(\frac{\nabla u}{|\nabla u|})$.

(10) is the final curve evolution equation, which can be implemented by level set method.

4. EXPERIMENTS

We design two groups of experiments in this section. In the first group, a 185*189 synthetic image is drawn to describe the real vessel branches, where a line-like hierarchy structure represents the vessel or other line-like structures. The gray value of line-like structure is 200 and the background is 128. See Fig. 2(1). The boundary of synthetic image is known. Next we design two groups of images based on the synthetic image for simulating the real vessel or other line-like images. The first group is noisy images. The noise is Gaussian random noise with zero mean and different standard deviation. The standard deviations of Fig. 2(2) to Fig. 2(5) are 35,55,85,105 respectively. The images in the second group are blurred images and different Gaussian templates are applied on them. From Fig. 3(1) to Fig. 3(5), the standard deviations of templates are 2, 3, 4, 5, 6.

Table 2. MAD in the segmented images.

	1	2	3	4	5
Fig. 2	0.153	0.2330	0.4486	0.8475	1.3356
Fig. 3	0.2451	0.4809	0.7326	1.3475	1.6120

We use the mean absolute distance(MAD) to compare the difference between the real boundary and the final contour obtained by the proposed method, i.e., (10), which represents the segmentation result. Supposing the real boundary A and contour B are represented at point sets, i.e., $A = \{a_1, a_2, \cdots, a_n\}$ and $B = \{b_1, b_2, \cdots, b_m\}$, the distance between them is defined by the MAD

$$e(A,B) = \frac{1}{2}\left\{\frac{1}{n}\sum_{i=1}^{n} d(a_i, B) + \frac{1}{m}\sum_{i=1}^{m} d(b_i, A)\right\},$$

where $d(a_i, B) = \min \|b_j - a_i\|$.

The first row of Table 2 indicates that the proposed multiscale model is robust to noise, and the

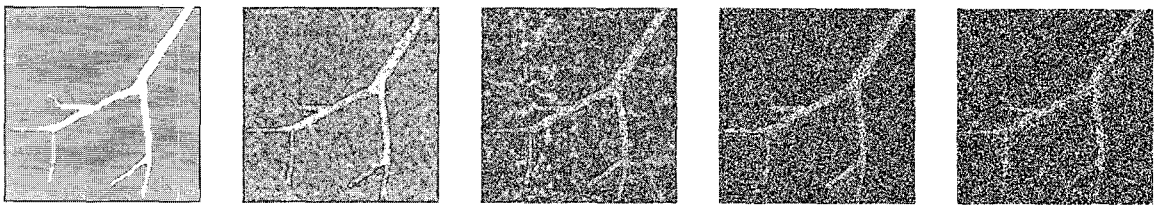

(1) (2) (3) (4) (5)

Fig. 2. Synthetic images with different noise.

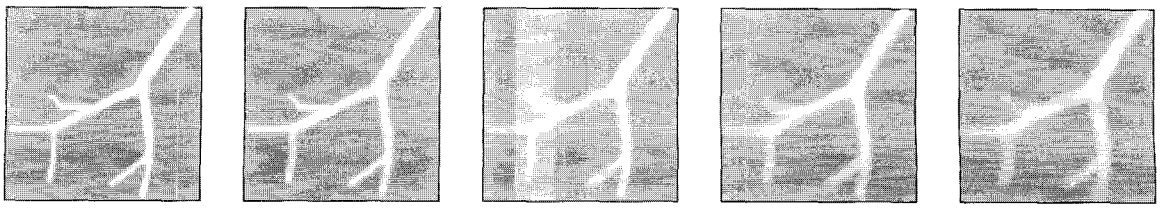

(1) (2) (3) (4) (5)

Fig. 3. Synthetic images with different gaussian smooth.

performance is reduced slowly when the noise is serious. Meanwhile, the MAD is increased smoothly, which proves that the model is steady with noise varying. See from the second row, the MAD in blurry images is bigger, which indicates that the algorithm performance in low contrastive images is worse than that in noise images. When the images are blurry, the segmented result is more possible to deviate from the real boundary. Therefore, it is necessary to increase the image contrast by any known enhancement methods before segmentation, which helps to improve the segmentation results.

To demonstrate our new vessel segmentation model, the proposed level set evolution equation (10) for vessel extraction is compared with other three conventional methods.

Experiment 1: Geodesic active contour model presented by Reference [13]:

$$\frac{\partial C}{\partial t} = g(|\nabla I|)(c_1 + c_2 k)\cdot \vec{N} - (\nabla g(|\nabla I|)\cdot \vec{N})\cdot \vec{N}.$$

In the following experiment, $c_1 = 1$, $c_2 = -0.1$. The values of c_1 and c_2 can work well in most images [13].

Experiment 2: The evolution equation presented by Malladi [7]:

$$\frac{\partial C}{\partial t} = g(|\nabla I|)\cdot(c - \varepsilon k) - \beta(\nabla P\cdot \vec{N})\cdot \vec{N},$$

where $P = -|\nabla G * I|$, $\vec{N}$ is outer normal vector, $c = 1$, $\varepsilon = 0.1$, $\beta = 0.1$.

Experiment 3: Fully global approach presented by Yezzi [10]:

$$\frac{\partial C}{\partial t} = (u - v)\cdot\left(\frac{I-u}{A_u} + \frac{I-v}{A_v}\right)\cdot \vec{N} - \beta\cdot k\cdot \vec{N},$$

where u, v are the average of interior or exterior intensity of the curve, A_u, A_v are interior and exterior area. We set $\beta = 0.1$ in the experiment.

Experiment 4 : The proposed model in this paper:

$$\frac{\partial u}{\partial t} = \alpha \times p(I(x,y,z))\cdot|\nabla u| + (1-\alpha)\left\{g(|\nabla I|)(c_1 + c_2 k)\cdot|\nabla u| - (\nabla g(|\nabla I|)\cdot \vec{N})\cdot|\nabla u|\right\},$$

where the best results are obtained for $\alpha = 0.5$, $c_1 = 1, c_2 = -0.1$. In most cases, α should be bigger than 0.5, because the vesselness measure is more efficient than gradient information in noise images. Moreover, the selection of big α makes the segmentation result not to be sensitive to the initial condition. The selection of c_1 and c_2 is similar to the first experiment.

In the following experiments, we present some segmentation results of 2D medical vessel image. All the methods can be extended to 3D medical image because they are implemented in level set framework. The medical image is pulmonary vessels selected from CT image. The obtained image is low contrast and accompanied by random noise, where many branches are blurry and discontinuous intensity. The first column shows the initial seed curves; the second and the third column show the random middle state of the curves; the fourth column shows the final segmentation result.

Fig. 4(1)-(4) are the results of geodesic active contours model, where the big vessel branches can be extracted successfully. However, many narrow or blurry branches are failed to be captured because the boundary-based information in these branches is too weak. The results of experiment 2 are Fig. 5(1)-(4). Like geodesic active contour model, the only boundary-based information is too weak to propagate the front in thin branches. Meanwhile, the boundary-based models are sensitive to the initial condition and all the seeds have to be set nearby branches. Another problem in these approaches is that the curves are easy to leak out of weak edges if the improper parameters are selected.

Fig. 6(1)-(4) are the results of Yezzi's model. It is not sensitive to the initial condition and all the seeds are set at random. Because it only uses the global intensity information in the evolution equation, many low contrastive pixels in vessels are excluded from ROI. Therefore, the result of the experiment is not satisfied. Fig. 6(4) shows the final result, where many thin branches are not captured successfully. Fig. 7(1)-(4) are the results of the proposed model in this paper, where the vessels, especially narrow thin branches, can be extracted successfully. Moreover, many blurry and even broken branches can be captured and connected automatically. Meanwhile, although the intensity of many branches is discontinuous, the vessel region information function is effective to find them. Fig. 7(4) shows the final result, which demonstrates the performance of our approach. It is very promising.

The computation time of the experiment 4 is about 16 seconds, where our computer is Intel Celeron 2.4G, 256M memory and the program is implemented in MATLAB. The computational time or iteration number depends on the initial location of seeds defined by the user. The iteration number is small if the initial seeds are defined near the boundary; otherwise the iteration number is very big. Therefore, it is not a good idea to define the seeds by users. We recommend that the initial seeds should include the pixels with big $v(x)$ as many as possible. In this case, the seeds are very close to the boundary. Here,

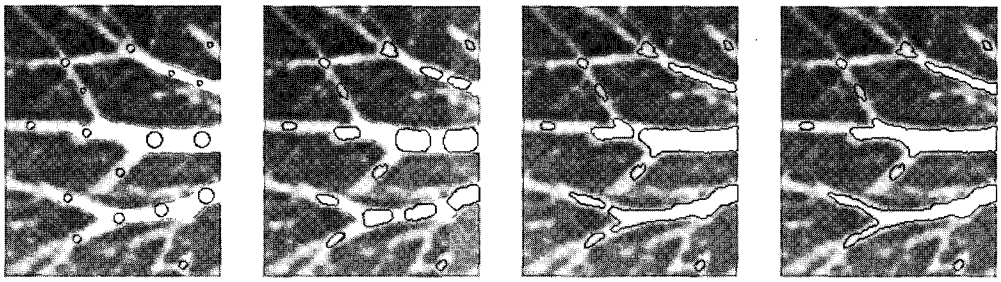

(1) (2) (3) (4)

Fig. 4. The experiment of Geodesic active contour model. (1) is the initial state. (2) and (3) are the middle states. (4) is the segmentation result.

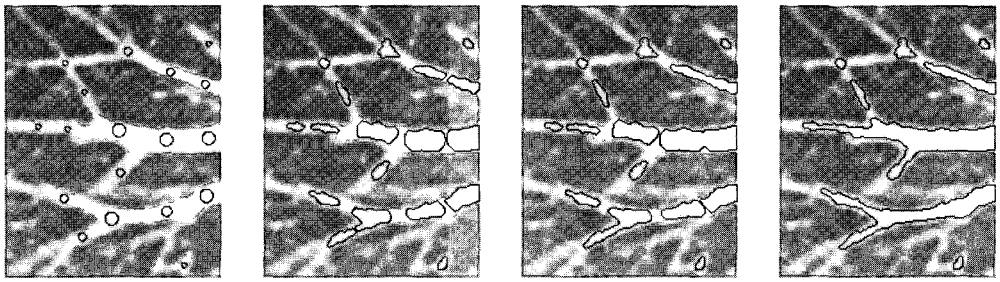

(1) (2) (3) (4)

Fig. 5. The experiment of Malladi's model. (1) is the initial state. (2) and (3) are the middle states. (4) is the segmentation result.

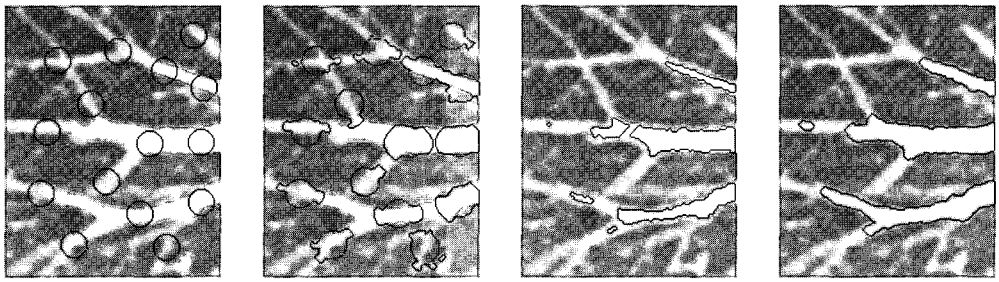

(1) (2) (3) (4)

Fig. 6. The experiment of Yezzi's model. (1) is the initial state. (2) and (3) are the middle states. (4) is the segmentation result.

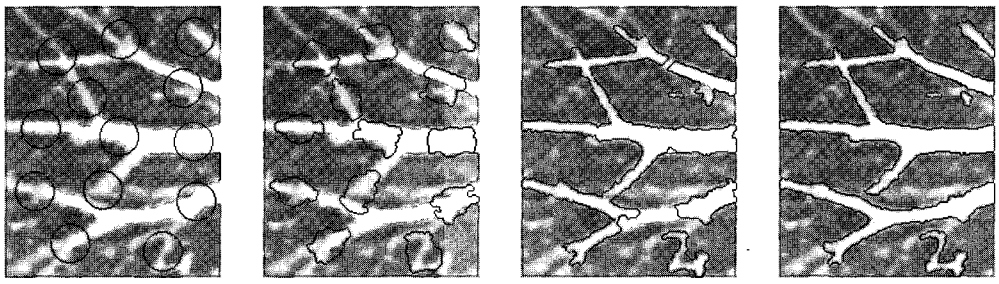

(1) (2) (3) (4)

Fig. 7. The experiment of the proposed model. (1) is the initial state. (2) and (3) are the middle states. (4) is the segmentation result.

we include the pixels with $v(x) > T$, where the threshold T is fixed to 0.5. The automatic method is easy to program and it reduces the iteration number. However, the prior information can't be applied in the conventional methods such as geodesic, Malladi or Yezzi's models.

5. CONCLUSION

In this paper, we proposed a novel efficient multiscale vessel segmentation method, which is based on level set framework. This method is not only efficient for the vessel segmentation, but also for other line-like structures. The vessel structure analysis is based on the multiscale enhancement filter. We defined a new vessel information function and a new region-based energy function. This method is not sensitive to the initial condition. A new curve evolution model is incorporated with the edge-based speed function. The proposed approach was implemented in the level set framework and is suitable for various topologic changes. Moreover, it can be easily extended to 3D images because the multiscale enhancement filter works well in 3D space. This approach was validated in human CT images for pulmonary vessel segmentation. Experiments show that the new method works better than the conventional snake models for the segmentation of narrow thin vessel branches.

APPENDIX A

According to variational theory and gradient descent method, we can acquire its evolution equation with minimizing E_{vessel}. For simplicity, we only provide the derivations in 2D space; it can be similarly extended to 3D. The detailed derivations are given as follows.

Firstly, we suppose:

$$E_{vessel} = -\iint_R p(I(x,y))dxdy = \iint_R f(x,y)dxdy,$$
$$Q = \frac{1}{2}\int_0^x f(t,y)dt, \quad P = \frac{1}{2}\int_0^y f(x,t)dt.$$

From Green formulation:

$$\begin{aligned} E_{Vessel} &= \iint_R (\frac{\partial P}{\partial y} + \frac{\partial Q}{\partial x})dxdy = \int_{\partial R} Qdy - \int_{\partial R} Pdx \\ &= \int_{\partial R} (Q\frac{dy}{ds} - P\frac{dx}{ds})ds \\ &= \int_0^L F(s, x(s), y(s), x'(s), y'(s))ds, \end{aligned} \tag{11}$$

where s is arc length parameter, and L is the curve length.

According to the variational theory, the Euler-Largrange of equation (11) is:

$$\begin{cases} F_x - \frac{d}{ds}F_{x'} = 0 \\ F_y - \frac{d}{ds}F_{y'} = 0 \end{cases} \Rightarrow \begin{cases} y'(s)\frac{\partial Q}{\partial x} - x'(s)\frac{\partial P}{\partial x} + \frac{dP}{ds} = 0 \\ y'(s)\frac{\partial Q}{\partial y} - x'(s)\frac{\partial P}{\partial y} - \frac{dQ}{ds} = 0. \end{cases} \tag{12}$$

Because

$$\begin{cases} \frac{dp}{ds} = x'(s)\frac{\partial P}{\partial x} + y'(s)\frac{\partial P}{\partial y} \\ \frac{dQ}{ds} = x'(s)\frac{\partial Q}{\partial x} + y'(s)\frac{\partial Q}{\partial y}. \end{cases} \tag{13}$$

Substitute (13) to (12)

$$\begin{cases} y'(s)\cdot(\frac{\partial Q}{\partial x} + \frac{\partial P}{\partial y}) = 0 \\ -x'(s)\cdot(\frac{\partial Q}{\partial x} + \frac{\partial P}{\partial y}) = 0 \end{cases} \Rightarrow \begin{cases} y'(s)\cdot f(x,y) = 0 \\ -x'(s)\cdot f(x,y) = 0. \end{cases}$$

From gradient descent method, the evolution equation is presented as:

$$\begin{cases} \frac{\partial x}{\partial t} = -f(x,y)\frac{dy}{ds} \\ \frac{\partial y}{\partial t} = f(x,y)\frac{dx}{ds}. \end{cases}$$

Because $\vec{T} = (\frac{dx}{ds}, \frac{dy}{ds})$ is unit tangential vector and $\vec{N} = (\frac{dy}{ds}, -\frac{dx}{ds})$ is the outer vector, the evolution equation can be defined as:

$$\frac{\partial C}{\partial t} = -f(x,y)\cdot\vec{N} = p(I(x,y))\cdot\vec{N}.$$

REFERENCE

[1] S. Chaudhuri, S. Chatterjee, N. Katz, M. Nelson, and M. Goldbaum, "Detection of blood vessels in retinal images using two dimensional matched filters," *IEEE Trans. on Medical Imaging*, vol. 8, no. 3, pp. 263-269, September 1989.

[2] B. D. Thackray and A. C. Nelson, "Semi-automatic segmentation of vascular network images using a rotating structuring element (ROSE) with mathematical morphology and dual feature thresholding," *IEEE Trans. on Medical Imaging*, vol. 12, no. 3, pp. 385-392, September 1993.

[3] M. Sonka, G. K. Reddy, M. D. Winniford, and S. M. Collins, "Adaptive approach to accurate analysis of small-diameter vessels in cineangiograms," *IEEE Trans. on Medical Imaging*, vol. 16, no. 1, pp. 87-95, February 1997.

[4] C. Yuan, E. Lin, J. Millard, and J. Hwang, "Closed contour edge detection of blood vessel lumen and outer wall boundaries in black-blood images," *Magnetic Resonance Imaging*, vol. 17, no. 2, pp. 257-266, February 1999.

[5] F. Zana and J. C. Klein, "A multimodal registration algorithm of eye fundus images using vessels detection and Hough transform," *IEEE Trans. on Medical Imaging*, vol. 18, no. 5, pp. 419-428, May 1999.

[6] J. A. Sechian, *Level Set Methods and Fast Marching Methods*, Cambridge University Press, England, 1999.

[7] R. Malladi, J. A. Sethian, and B. C. Vemuri, "Shape modeling with front propagation: A level set approach," *IEEE Trans. on Pattern Analysis and Machine Intelligence*, vol. 17, no. 2, pp. 158-175, February 1995.

[8] A. F. Frangi, W. J. Niessen, K. L. Vincken, and M. A. Viergever, "Multiscale vessel enhancement filtering," *Lecture Notes in Computer Science*, vol. 1496, pp. 130-137, 1998.

[9] P. Nikos, "Geodesic active regions: A new framework to deal with frame partition problems in computer vision," *Journal of Visual Communication and Image Representation*, vol. 13, pp. 249-268, 2002.

[10] A. Yezzi, A. Tsai, and A. Willsky, "A fully global approach to image segmentation via coupled curve evolution equations," *Journal of Visual Communication and Image Representation*, vol. 13, pp. 195-216, 2002.

[11] M. Pascal, R. Philippe, G. Francois, and G. Prederic, "Influence of the noise model on level set active contour segmentation," *IEEE Trans. on Pattern Analysis and Machine Intelligence*, vol. 26, no. 6, pp. 766-803, June 2004.

[12] G. Ali and C. Raphael, "A new fast level set method," *Proc. of the 6th Signal Processing Symposium*, pp. 9-11, 2004.

[13] V. Caselles, R. Kimmel, and G. Spairo, "Geodesic active contours," *International Journal of Computer Vision*, vol. 22, pp. 61-79, 1997.

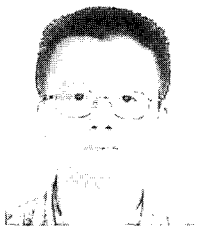

Gang Yu was born in 1975. He is currently a Ph.D. candidate at the School of Life Science and Technology, Xi'an Jiaotong University, China. He received the B.S. degree in printing engineering from Xi'an University of Technology in 1998, and the M.S. degree from Xi'an University of Technology in the area of computer science in 2002. His research interests are the theory and technology of medical image segmentation and fusion.

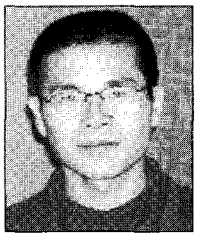

Pan Lin is a Lecturer with the Faculty of software at Fujian Normal University. His research interests include medical image processing, computer vision, pattern recognition, software engineering and their applications.

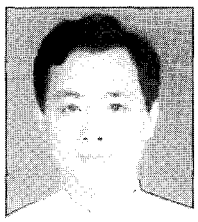

Peng Li is a doctor candidate in Xi'an Jiaotong University, China. His research interest is medical signal processing.

Zhengzhong Bian is a doctor supervisor in Xi'an Jiaotong University. His research interests include medical information processing and remote medicine.